J Mater Sci (2007) 42:1709–1727
DOI 10.1007/s10853-006-0700-9

Strain rate effects in the ultrafine grain and nanocrystalline regimes—influence on some constitutive responses

Q. Wei

Received: 22 May 2006 / Accepted: 21 July 2006 / Published online: 13 January 2007

Abstract Mounting evidence is pointing to some emerging novel behaviors of metals with ultrafine-grain (UFG) and/or nanocrystalline (NC) microstructures. One such novel behavior is related to the thermodynamic and kinetic aspects of plastic response in the UFG/NC regime. Two inter-related parameters, viz., the strain rate sensitivity (SRS) and the activation volumes of plastic deformation, are used as fingerprints for the thermodynamics and kinetics of plastic deformation. Changes of these parameters with grain size may indicate transition of plastic deformation mechanisms. Therefore, investigations of these phenomena may bring out new strategies for ingenious design and synthesis of UFG/NC materials with desirable properties. In this article, we present a critical review on the experimental results and theories associated with the SRS of UFG/NC metals with different lattice structures, and the influences on some constitutive responses.

Introduction

High strength has been the paramount requirement for metallic materials in structural applications. Among the technical routes to elevate the strength of metals, grain refinement or microstructure refinement claims a long and outstanding history. The best known effect is summarized into the relationship derived by Hall and Petch in the 1950s [1, 2], which predicts that the yield strength or flow stress of a metal is proportional to the inverse square root of the grain size, i.e.,

$$\sigma_y = \sigma_0 + k_{\mathrm{H-P}} \cdot d^{-1/2}, \tag{1}$$

where σ_0 is due to lattice friction, $k_{\mathrm{H\text{-}P}}$ the Hall–Petch slope, and d the grain size. A number of mechanisms have been proposed to explain the Hall-Petch relationship, including pile-up of dislocations against the grain boundaries (GBs) [3], grain boundaries acting both as dislocation sources and sinks [4], and presence of geometrically necessary dislocations (GNDs) in the vicinity of the grain boundaries to account for the deformation compatibility of polycrystalline metals [5]. These mechanisms, while based on different physical pictures, share the popularity in the community. Break-down of the Hall-Petch relationship when the grain size is refined into the nanometer regime (d a few tens of nm) was frequently reported during late 1980s–1990s [6–11]. On retrospection, that is probably part of the reason for the burgeoning interest in metals and alloys with nanocrystalline microstructures during the past two decades.

The technical routes to produce ultrafine grained (UFG, grain size $d < 500$ nm but > 100 nm) and NC ($d < 100$ nm) metals can be classified into two categories [12]. The first is the bottom-up method where powders of nanometer particles are synthesized via various techniques and then compacted into bulk forms, similar to conventional powder metallurgy (PM). The second is the top-down method where grain

Q. Wei (✉)
Department of Mechanical Engineering and Engineering Science, University of North Carolina at Charlotte, 9201 University City Blvd., Charlotte, NC 28223-0001, USA
e-mail: qwei@uncc.edu

size of a bulk metal is refined into the UFG/NC regime, by means of, for example, severe plastic deformation (SPD) [13]. A longstanding concern associated with UFG/NC metals is their diminished tensile ductility, an issue which has been believed to be largely due to volume defects such as porosity and impurity contamination from the bottom-up routes. A number of strategies have been exploited to lift the ductility concern in the UFG/NC regime. An excellent commentary in this respect is given by Professor Ma who has summarized the eight possible strategies to enhance tensile ductility of UFG/NC metals [14]. Such strategies may be based on microstructure engineering in a broad sense, or they may be based on certain new properties revealed recently for UFG/NC metals. One such new property is associated with the strain rate effect on the strength of UFG/NC metals. Experimental evidence has indicated that when the grain size of face-centered cubic (FCC) metals is refined, their strength exhibits increased dependence on strain rate [15]. This effect is even more pronounced in the UFG/NC regime [11, 16–29]. Body-centered cubic (BCC) metals show the opposite trend, viz. strain rate dependence of their strength decreases with reduction in grain size [11, 17, 30–36]. Grain size effect on the strain rate dependence of the strength of hexagonal close-packed (HCP) metals was investigated in the 1960s and 1970s [37–40], but the grain size was not extended into the UFG/NC regime at the time. Recently a very limited number of papers have been published on HCP metals in terms of strain rate effects in the UFG/NC regime [41–46].

Constitutive response of a material is usually represented in a functional form in terms of strain rate (or deformation rate) under certain conditions. For example, the following equation is used to describe the constitutive behavior according to Kocks and coworkers [47]

$$\dot{\varepsilon} = f(P, T, \sigma, \dot{\sigma}, s_1, s_2, \ldots), \tag{2}$$

where $\dot{\varepsilon}$ is the strain rate, P the pressure, T the temperature, σ the applied stress; $\dot{\sigma}$ is the rate of change of the stress, s_1, s_2,... the internal structural variables such as grain size, mobile dislocation density, forest dislocation density, etc.

While strong and consistent evidence has suggested novel phenomena in terms of grain size effect on strain rate dependence of strength in the UFG/NC regime, yet interpretation of the experimental evidence is quite intriguing at this point. Discussions of the impact on the constitutive responses of UFG/NC metals are only sporadic. Consistent and plausible theories and models are still lacking. All these call for further effort to address the grain size effect on the strain rate dependence in the UFG/NC regime.

A few years back, this author and co-workers and a few other groups presented some definite experimental results on the strain rate effects in the UFG/NC regime for FCC and BCC metals [17, 23, 25, 26]. They also tried to give some preliminary theoretical reasoning. Many more papers have been published since then [20, 24, 48–53], including the application of nano-indentation to probe the rate effect of NC metals [48], and attempt for dislocation based models [54]. In a very recent comprehensive and excellent review article on mechanical properties of nanocrystalline metals, Meyers et al., provide a brief summary in light of the strain rate effects in the UFG/NC regime [11]. Due to the scope of their review, collection of experimental data regarding the strain rate effects in the UFG/NC regime is not inclusive. An in-depth discussion about the underlying mechanisms associated with such phenomena is needed. The link between the novel strain rate effects and the constitutive responses of UFG/NC metals should be elaborated. Therefore, we believe the undertaking of a critical and focused review on this important issue is now timely. In this overview, we will present a baseline summary of the state-of-the-art experimental results and some theoretical frameworks on the strain rate effects in the UFG/NC regime, and how they will influence some of the constitutive behavior of UFG/NC metals. Outstanding issues and future directions will also be noted.

A concise theoretical formulation of the strain rate effect in plastic deformation of metals

At high homologous temperatures ($T/T_m > 0.4$, for example), plastic deformation of metals under a certain applied stress takes place through various mechanisms of creep, which is a well known thermally activated process. The steady-state creep rate can be described by an Arrhenius-type equation as

$$\dot{\varepsilon}_S = K\sigma^n \exp(-\frac{Q_C}{kT}), \tag{3}$$

where $\dot{\varepsilon}_S$ is the steady state creep rate, K a constant, σ the applied stress, n the stress exponent, Q_C the activation energy for creep, k the Boltzmann constant and T the absolute temperature. Evaluation of n and Q_C and comparison of their values with theoretical models shed light on the specific mechanisms of creep.

Thermal fluctuation is an omnipresent phenomenon in a material system as long as the temperature is above 0 K [47]. Therefore, plastic deformation of metals via the dislocation-mediated mechanisms in general can also be a thermally assisted process. In other words, thermal fluctuation can assist the applied stress in surmounting obstacles to plastic flow, though the temperature dependence is a function of lattice type, type of obstacles and the particular dislocation mechanism involved. In view of this, the shear strain rate, $\dot{\gamma}$, can be given by an Arrhenius-type equation as,

$$\dot{\gamma} = \dot{\gamma}_0 \exp(-\frac{\Delta G(\tau^*)}{kT}), \tag{4}$$

where the pre-exponential factor $\dot{\gamma}_0$ includes the number of possible activation sites, the average shear strain per successful thermal fluctuation, and the frequency of the vibration of the elemental unit involved in the thermal activation. ΔG is the activation energy and is usually a strong function of the shear stress component τ*, viz. the net shear stress resolved to drive the dislocation mechanism. This shear stress component is itself defined by $\tau^* = \tau_a - \tau_\mu$, where τ_a is the applied shear stress and τ_μ is the athermal internal stress stemming from long-range obstacles such as grain boundaries, secondary phases, etc. For more general stress states, the net shear stress τ* is replaced by the effective stress $\tau_e = \sqrt{(1/2)S_{ij}S_{ij}}$, with S_{ij} being the components of the deviatoric stress tensor, and the shear rate $\dot{\gamma}$ is replaced by the work-conjugate effective plastic strain rate $\bar{\dot{\gamma}}^p$.

The above formulation is based on the assumption that plastic deformation is from the single slip of dislocations in a lattice. For polycrystalline metals under uniaxial tensile or compressive stress, the Taylor factor may be used to convert the uniaxial stress, σ into the shear stress component. That is, $\tau_a = \sigma / M$, where the Taylor factor M is usually around 3.0.

According to the von Mises yield theory, the yield shear stress is $\tau_Y = \sigma_Y/\sqrt{3}$ (σ_Y is the uniaxial yield stress), and the equivalent plastic shear strain is $\gamma^p = \sqrt{3} \cdot \varepsilon^p$ (ε^p is the uniaxial strain). The activation energy can be written into two parts as

$$\Delta G = \Delta G^* - \tau^* \cdot v^*, \tag{5}$$

where the first term on the right hand side represents the activation energy needed to be provided by thermal activation alone (in the absence of any applied stress), and v^* is the activation volume. Apparently, the activation volume can be written as the derivative of the activation energy with respect to the effective shear stress, i.e.,

$$v^* = -\frac{\mathrm{d}(\Delta G)}{\mathrm{d}\tau^*}. \tag{6}$$

From Eq. (4), therefore, we can write

$$v^* = kT(\frac{\partial \ln \dot{\gamma}}{\partial \tau}). \tag{7}$$

To reach the above equation for the activation volume, assumption is made that the athermal part of the shear stress is a constant, which turns out to be true in general for a constant internal structure. This equation can be re-written as

$$v^* = \frac{kT}{\tau} \cdot \frac{\partial \ln \dot{\gamma}}{\partial \ln \tau}. \tag{8}$$

Finally, if we define

$$m = \frac{\partial \ln \tau}{\partial \ln \dot{\gamma}}, \tag{9}$$

we can write the activation volume as

$$v^* = \frac{kT}{\tau \cdot m}. \tag{10}$$

The parameter, m, is the experimentally measured "strain rate sensitivity," or SRS. It is an important factor in determining the constitutive response of materials. Based on Eq. (10), we can have

$$m = \frac{kT}{\tau \cdot v^*}. \tag{11}$$

Here we see the close inter-relation between the SRS and the activation volume of plastic deformation. It is obvious that the SRS can be equally written in terms of uniaxial stresses and strains such that

$$m = \frac{\partial \ln \sigma}{\partial \ln \dot{\varepsilon}}. \tag{12}$$

However, if the SRS is written in terms of the activation volume and the applied uniaxial stress, the von Mises relation should be used such that

$$m = \frac{\sqrt{3}kT}{\sigma \cdot v^*}. \tag{13}$$

Recently, instrumentation nanoindentation has been used by a number of groups to derive the SRS of UFG/NC metals. In this case, the classical Tabor relation can be used (the yield strength of a metal is roughly one third of its nanoindentation hardness or microhardness, i.e., $H = 3 \cdot \sigma_s$). Consequently, we can assess the SRS as

$$m = 3\sqrt{3}\frac{kT}{H \cdot v^*}. \quad (14)$$

The activation volume is determined by the mechanism responsible for the plastic deformation. Some investigators prefer to use the activation area, A^*, which is related to the activation volume by

$$v^* = A^* \cdot b, \quad (15)$$

where b is the strength (or magnitude) of the Burgers vector of dislocations. The activation volume is often given in terms of b^3. A wealth of data is available in the literature regarding the SRS and activation volumes of single crystal or coarse-grained (CG) FCC and BCC metals, and some HCP metals [55–57].

Experimental results on strain rate sensitivity of ultrafine grained and nanocrystalline metals

A variety of experimental techniques have been used to assess the thermodynamic and kinetic aspects of plastic deformation of metals. Strain rate jump tests at a constant temperature, either under compression or tension, are amongst the most widely used method. In this experiment, the imposed rate of deformation of the specimen is changed by changing the speed of the cross-head of the testing system. A basic assumption for such experiment is that the internal structure such as mobile dislocation density is not changed by changing the rate of plastic deformation. Up-jumps where abrupt increases in the cross-head speed are imposed are preferred to avoid complexity introduced by the system compliance. Extraction of SRS from such experiment is straightforward by using the following equation

$$m = \frac{\Delta \ln \sigma}{\Delta \ln \dot{\varepsilon}}, \quad (16)$$

where $\Delta \ln \sigma = \ln \sigma_2 - \ln \sigma_1$, and σ_2 and σ_1 correspond to the measured flow stresses after and before the imposed rate change; $\Delta \ln \dot{\varepsilon} = \ln \dot{\varepsilon}_2 - \ln \dot{\varepsilon}_1$, and $\dot{\varepsilon}_2$ and $\dot{\varepsilon}_1$ are the imposed strain rates. (It should be noted that for a strain hardening material, the flow stress is a function of strain, and the m value should be given along with the specific strain level at which it is derived. This is more of a concern for FCC metals and some HCP metals. But it is less of a concern for most BCC metals since their stress-strain curves at different temperatures or under different strain rates are almost parallel.) Another experimental technique involves stress relaxation or load relaxation. In such an experiment, the specimen is mechanically strained into the plastic regime, and then the cross-head of the testing system is arrested. The data acquisition system records the stress as a function of time. For a hard machine with infinite stiffness, the total strain rate will be zero,

$$\dot{\varepsilon}_e + \dot{\varepsilon}_p = 0, \quad (17)$$

where $\dot{\varepsilon}_e, \dot{\varepsilon}_p$ are the elastic strain rate and plastic strain rate from the specimen. However, a hard machine with infinite stiffness is unrealistic and removal of the system compliance is often quite involved. An alternative way is to plot $\ln\dot{\sigma}$ versus $\ln\sigma$, and SRS can be calculated as [58, 59]

$$m = \frac{d\ln\sigma}{d\ln\dot{\sigma}}. \quad (18)$$

Experimental results have shown that SRS obtained by stress relaxation exhibit consistent agreement with those from other experiments [60].

High strain rate (dynamic) behavior can be evaluated by means of stress-wave techniques such as split Hopkinson pressure bar (SHPB) systems [61]. With such techniques, well characterized, uniaxial strain rates up to $10^4 s^{-1}$ can be achieved routinely.

In this section, we will present a digest of experimental data on the strain rate effects in the UFG/NC regime according to the lattice structure of the metals.

FCC Metals

In 1953, Carreker and Hibbard reported the first experimental observation of enhanced strain rate effect on plastic behavior of pure Cu through grain size reduction [15]. They showed that SRS of high purity Cu increased from 0.004 (large d) to 0.0072 (small d). But the d range of their work was in the CG regime (from 12 μm to 90 μm). Recently, numerous papers have reported enhanced SRS in UFG/NC metals with FCC lattice (Refs. [15, 17, 18, 20, 48, 53, 62–69] for Cu; Refs.[16, 24, 60, 64, 65, 70, 71] for Ni; Ref. [51, 55, 72–75] for Al). The UFG/NC metals have been produced by various technical routes, including powder metallurgy, electrodeposition and severe plastic deformation (SPD). The general observation is that the SRS of FCC metals increases regardless of the technical routes used to produce the metals.

For example, Torre et al. [53] have studied the SRS as a function of grain size for a pure copper. The SRS was measured by strain rate jump tests under compression at room temperature. The UFG microstructure was achieved via equal channel angular pressing

(ECAP) by 0, 1, 2, 4, 8, 12 and 16 passes, respectively. During ECAP, the apparent grain size saturates quickly after about 2 passes. However, as pointed out by Valiev et al.[63], the fraction of large-angle grain boundaries continues to increase and the microstructure becomes more homogeneous with increased ECAP passes. Therefore, the effective grain size defined by large-angle grain boundaries should be further refined with increased ECAP processing after the apparent grain size is saturated. They show that the SRS of pure Cu is significantly increased with reduced grain size.

Zehetbauer and Seumer [76] show that the activation volume for plastic deformation of pure copper decreases with increased shear stress (or plastic shear strain). (We should point out that their definition of strain rate sensitivity is $m = (d\ln\dot{\gamma})/(d\ln\theta)$, θ being the strain hardening rate. This definition is different from the commonly used SRS). One may argue based on Eq. (11) that the SRS should increase if the stress (or the effective stress component) is not changing [68]. Zehetbauer and Seumer did show that after Stage IV, the strain hardening parameter exhibits a plateau with increased stress, but the activation volume continues to decrease.

Chen et al. [48], used nanoindentation to investigate the loading rate sensitivity of hardness of pure Cu with different grain sizes. They produced NC Cu by magnetron sputtering of Cu onto substrates at different temperatures to control the grain size. They also employed surface mechanical attrition (SMA) to make a thin layer of NC Cu, and ECAP to make bulk Cu with UFG microstructure. Figure 1 displays their strain rate sensitivity versus grain size derived from nanoindentation measurement on Cu. The results of Chen et al. [48] agree qualitatively with those of Torre et al. [53], in that when the grain size is refined, the SRS of Cu increases.

In Fig. 2 we plot the literature data of SRS versus grain size for Cu. It should be noted here that two groups reported extraordinarily high SRS for UFG or NC Cu. The first is an SRS value of 0.14 from Valiev et al. [63], on Cu of 100 nm grain size produced by SPD, and the second is an SRS value of 0.104 from Jiang et al.[69], on Cu of 26 nm grain size produced by electric brush plating. In Fig. 2, the data points from these two groups are indicated by arrows to show they are off the scale in the plot. It should also be noted that the data points from Lu et al. [68] are based on Cu with no twins, with a low density of twins and with a high density of twins, respectively. Therefore, the grain size in the plot (500 nm) for all three microstructure does not account for the existence of twins. They pointed out that nano-sized twins enhance the SRS of Cu in the same way as the reduced grain size enhances SRS.

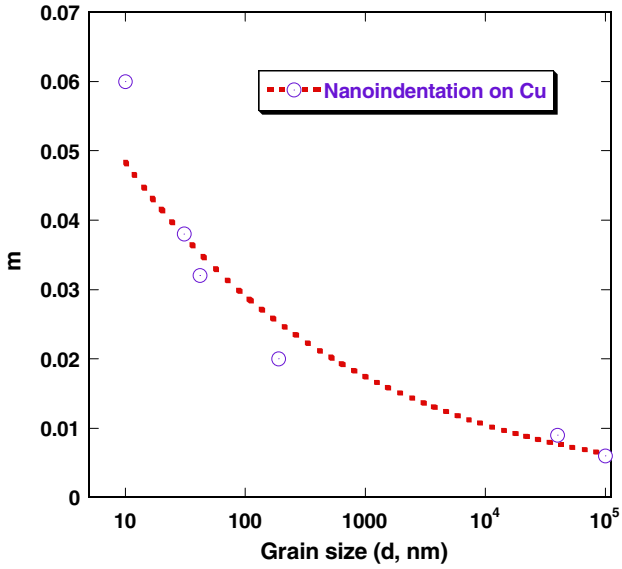

Fig. 1 Strain rate sensitivity of Cu as a function of grain size. The data points are extracted from the work of Chen et al. [48]. The m values are derived from nanoindentation measurements on Cu specimens with different grain sizes

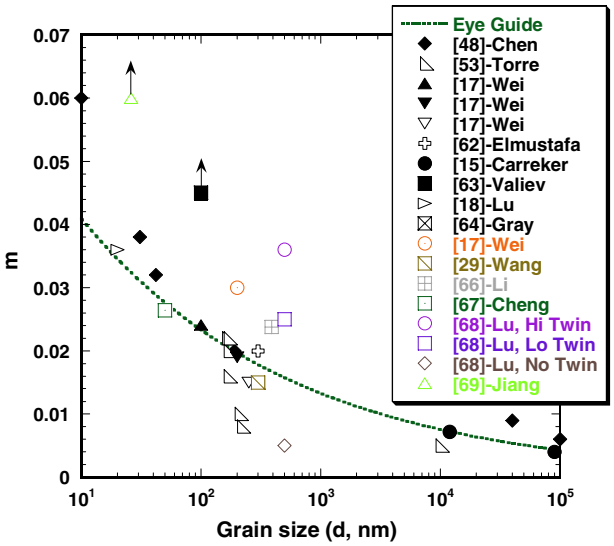

Fig. 2 Strain rate sensitivity of Cu as a function of grain size. The reference and its first author corresponding to each data point are also given in the plot. Two unusually high SRS values, one due to Valiev et al. [63], another due to Jiang et al. [69], are indicated by two upward arrows to show they are off the scale of the plot. The data points from Lu et al. [68] correspond to three densities of twins within the materials, i.e., high twin density, low twin density and absence of twin (No Twin)

Some experimental results exist for the SRS of Ni as a function of grain size. The UFG/NC nickel has been produced by electrodeposition or SPD. Figure 3

displays the results from different groups. The SRS of Ni as a function of grain size exhibits a trend very similar to that of Cu, whatever processing routes or testing methods are used to derive the experimental results shown in Fig. 3.

Another FCC metal that has been widely used as a structural material is aluminum. A few reports have become available only until recently [51, 55, 72–75]. Figure 4 has collected the data in the literature on SRS of Al as a function of grain size. It shows that Al, like Cu and Ni, has similar behavior. In this plot, the data point of Kalkman et al. [74], is derived via Eq. (11) using their experimental results of activation volume and flow stress of NC Al thin film specimens.

In summary, all the available literature data of the three representative FCC metals, i.e., Cu, Ni and Al show enhanced strain rate sensitivity when their grain size is refined into the UFG/NC regime.

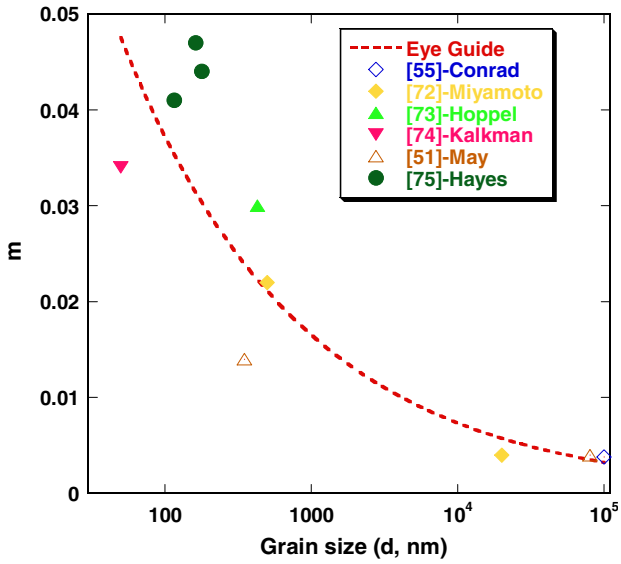

Fig. 4 Strain rate sensitivity of Al as a function of grain size. The reference and its first author corresponding to each data point are also given in the plot

BCC metals

The most popular BCC metal is Fe. Jia and co-workers [35] performed systematic experiments on the effect of grain size on the constitutive behavior of Fe. They used ball-milling to produce nanocrystalline Fe powders, and then used a two-step consolidation process at different temperatures to obtain fully dense Fe samples with different grain sizes. They investigated the mechanical behavior of the Fe samples from quasi-static to dynamic strain rates (~$10^3 s^{-1}$). They found that SRS of Fe decreased with reduced grain size. Figure 5 displays the SRS of Fe against grain size derived from the paper of Jia et al. [35]. Subsequent work on SPD Fe shows the same trend [33]. Malow and co-workers even reported negative SRS for NC ($d \sim 20$ nm) Fe produced in a way similar to that of Jia et al. [77]. A very high value of SRS was measured using nanoindentation on NC Fe particles ($d < \sim 10$ nm) by Jang et al. [36, 78]. However, some uncertainties have to be clarified regarding nanoindentation on powder samples

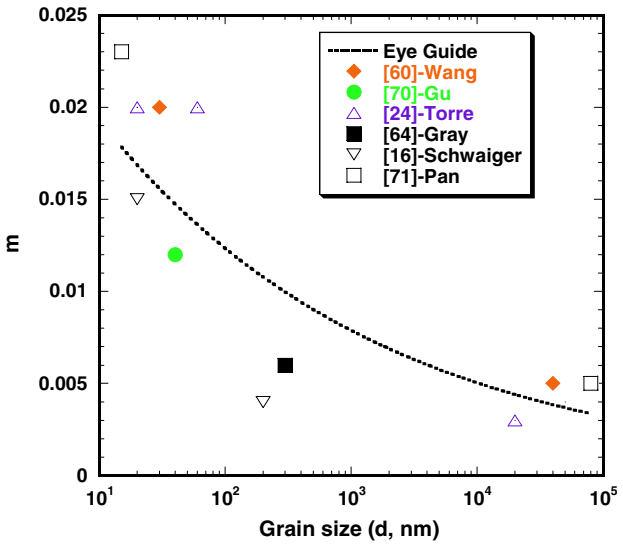

Fig. 3 Strain rate sensitivity of Ni as a function of grain size. The reference and its first author corresponding to each data point are also given in the plot

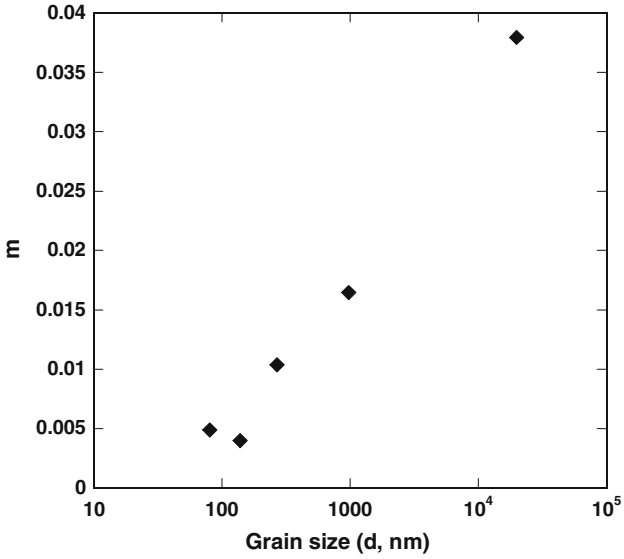

Fig. 5 Strain rate sensitivity of consolidated Fe as a function of grain size. The data points are extracted from the paper of Jia et al. [35]

and the unusually low m (0.006) obtained by the same authors for their coarse-grained Fe.

Recently, more work has been reported on mechanical behavior of other UFG/NC metals with BCC structure, such as Ta, V and W [30–32, 34, 79, 80]. In Fig. 6 we have plotted the SRS data of BCC metals against grain size. The general trend is apparent: the strain rate sensitivity of BCC metals decreases with reduced grain size. This trend is sharply opposing that of FCC metals as presented in Figs. 2–4. We should point out that the solid curve in Fig. 6 is based on the constitutive model for BCC metals proposed by Jia et al. [35].

HCP metals

Only a limited number of papers are available in the literature addressing the grain size effect on the SRS of HCP metals. A recent paper by Jia et al. [41] on commercial purity Ti showed that when the grain size is refined into the UFG regime ($d \sim 260$ nm), the SRS was reduced from ~0.04 of CG-Ti to ~0.025. The only data for CG-Co is by Karimpoor and co-workers [46] who measured a negative SRS for Co of ~5 μm in grain size, while for the NC-Co ($d \sim 12$ nm), the SRS is increased to ~0.012. Wang reported a SRS of ~0.025 for electrodeposited NC-Co ($d \sim 20$ nm) [65]. However, it is premature at this point to conclude whether grain size reduction increases the SRS of Co, due to the lack of reliable experimental results. Zhang et al., performed systematic work on in situ consolidated NC–Zn and measured a SRS of 0.15 at room temperature for d around 200 nm [43]. This value is much larger than that of the coarse-grained Zn obtained by Sastry [81] (m~0.057 for d = 4μm). The SRS derived from early results of Dorn and Mitchell [56] of single crystal Mg is around 0.041. Worthy of mention is that this is based on the basal slip mechanism for Mg. Creep tests on single crystal Mg by Conrad and co-workers at room temperature gave an SRS of ~0.19 [82]. Hwang et al., measured the SRS for NC-Mg (d = 45 nm) to be 0.6 at room temperature[42]. Trojanova and co-workers [83] measured the SRS for NC-Mg (d = 100 nm) to be ~0.31 at room temperature. It then suggests that the SRS of Mg may be increased by reduced grain size. The very high room temperature SRS is probably expected even for coarse grain Zn or Mg due to their very low melting point (T_m = 923 K for Mg and 692 K for Zn). For these two metals, increased SRS with decreased grain size may be attributed to enhanced grain boundary diffusion which contributes to plastic strain in the form of Coble creep at room temperature. Figure 7 displays the SRS of some HCP metals. In this plot, we used two upward arrows to indicate that the

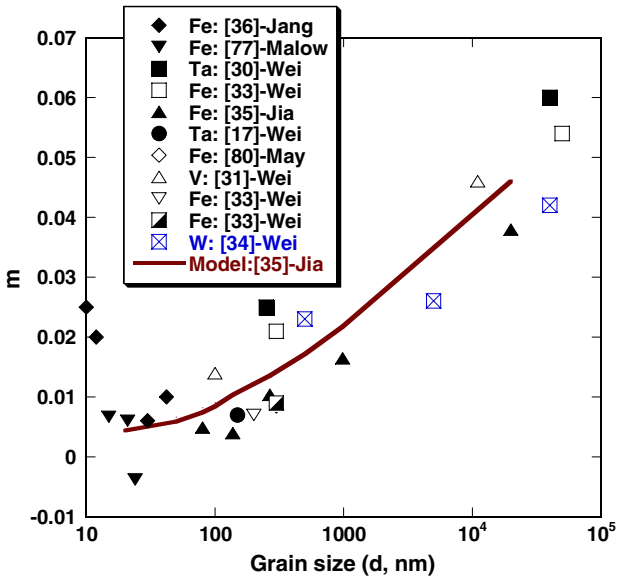

Fig. 6 Strain rate sensitivity of BCC metals. The grain size was refined by different methods, including ball milling followed by consolidation, severe plastic deformation, ECAP plus low temperature rolling, etc. The name of each metal is given in the inset, followed by the reference and its first author. The solid curve is the calculation result based on the model presented in Ref. [35]

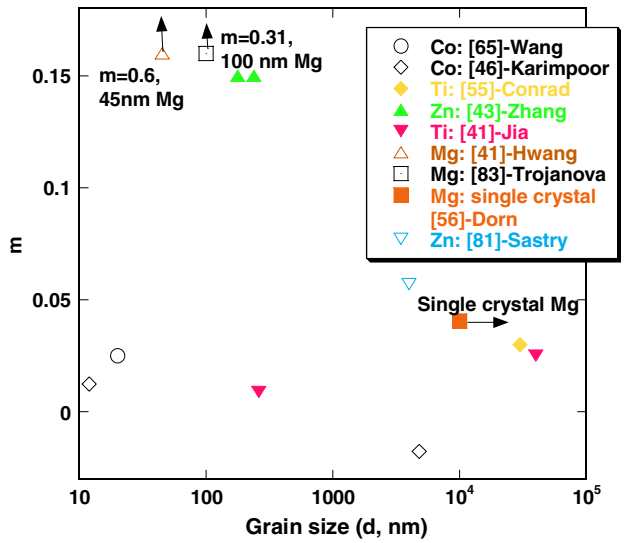

Fig. 7 Strain rate sensitivity of HCP metals as a function of grain size. The name of each metal is given in the inset, followed by the reference and its first author. The two very high SRS values for nanocrystalline Mg are marked by two upward arrows to indicate they are off the scale of the plot. The data point for single crystal Mg (solid square) is marked by a horizontal right-pointing arrow to show the grain size is off the scale of the plot

results of NC-Mg measured by Hwang et al. [42] and Trojanova et al. [83] are off the scale of the plot. The values of SRS are given in the plot. The data for single crystal Mg based on the results of Dorn and Mitchell [56] is indicated by a horizontal arrow pointing to the increasing direction of grain size. For the time being, any hypothesis is questionable about the grain size effect on SRS for HCP metals due to the extreme paucity of experimental results.

Theoretical models of strain rate sensitivity of ultrafine grained and nanocrystalline metals

In this section, we will first briefly review the dislocation mechanisms in terms of the rate controlling processes in single crystal or coarse-grained metals. Then we will proceed to discuss the connection between these mechanisms and the grain size effect on constitutive behavior of metals with different lattice structures. The link between the thermal and rate effect on the Hall–Petch relationship, particularly the Hall–Petch coefficient will be alluded to. Special attention will be drawn to the correlation between the indirect fingerprint of activation volume and the directly measured strain rate sensitivity.

Rate controlling processes in single crystal or coarse-grained metals

Annealed single crystal or coarse-grained FCC metals with low dislocation density have very insignificant strain rate dependence of yield strength (SRS ~0.004 for most single crystal or coarse grained FCC metals). However, their strain hardening is a strong function of temperature and strain rate, and as a consequence, the fracture behavior, including the tensile elongation to failure and fracture strength, depends strongly on temperature and strain rate. That implies glide of dislocations in an FCC lattice in the absence of foreign obstacles does not involve thermal activation. Since strain hardening of FCC metals involves intersections of forest dislocations and cross slip, and both processes can be thermally assisted, it is then expected that after yielding (or after the ''easy glide'' stage in single crystals), the rate controlling mechanisms in the plastic deformation of FCC metals are cutting of forest dislocations and cross slip. Both mechanisms play decisive roles in the dislocation pattern formation in FCC metals (see, for example, Ref.[84]). Because ease of cross slip depends critically on the stacking fault energy (γ_{SF}), it is natural to believe that stacking fault energy should play an important role in the kinetics of plastic deformation of FCC metals. For example, when a full dislocation is dissociated into two partials and a stacking fault ensues, the equilibrium splitting width between the two partials is[85]

$$r = a^2 \frac{\mu}{24\pi\gamma_{SF}}, \tag{19}$$

where a is a constant, and μ the shear modulus. Equation (19) indicates that the splitting width between two partials is inversely proportional to the stacking fault energy. During thermal activation, the splitting width will in turn determine the activation distance and accordingly the activation volume. One should thus expect the activation volume of plastic deformation of FCC metals a function of stacking fault energy. This has been ascertained, for example, by evaluating the activation volumes of Al and Cu [55]. In the FCC family, Al has the highest γ_{SF}, and experiments show that v^* of Al is much smaller than that of Cu at the same temperature and strain.

Another important observation regarding the plastic deformation of single crystal or coarse-grained FCC metals is that the Cottrell–Stokes law is generally obeyed for plastic strain over 10%. (The Cottrell–Stokes law predicts that for a given temperature change the ratio of flow stresses at two temperatures is roughly a constant [86]). In other words, if the applied shear stress is decomposed into the thermal component (τ^*) and the athermal component (τ_μ), the ratio τ^*/τ_μ is almost a constant. One more interesting observation is that both the thermal and athermal stresses obey the Hirsch-Bailey relation[87],

$$\tau \propto \mu b \rho^{1/2}, \tag{20}$$

where ρ is the dislocation density. This observation suggests that the mechanisms controlling the thermal stress and the athermal stress evolve in a similar manner during plastic deformation. In fact, Basinski proposes that the forest dislocations in FCC metals are the source for the long range athermal stress (τ_μ) as well as the short range thermal stress (τ^*) [88]. Narutani and Takamura [89] also provided evidence for nickel that the activation volume decreases with strain, supporting dislocation intersection as the rate controlling mechanism. They also observed that the activation volume decreases with decreased grain size.

Both experiments and theoretical simulations have corroborated that at low temperatures, the rate controlling mechanism in single crystal or CG-BCC metals is completely different from that in FCC metals. First of

all, the yield strength and flow stress of BCC metals are very sensitive to strain rate and temperature (SRS of single crystal or CG-BCC metals is usually one order of magnitude larger than that of FCC metals). Microstructural observations (via transmission electron microscopy (TEM), for example) on BCC metals upon finite plastic deformation reveal long and straight screw dislocations [90, 91]. It is postulated that the low mobility of the screws in BCC metals is the rate controlling factor in plastic deformation. This low mobility is rooted in the non-planar core structure of the screws, which entails a strong Peierls–Nabarro (P–N) barrier opposing the motion of screws [92]. As a consequence, the motion of screws in a BCC lattice is facilitated by the double-kink mechanism where by means of thermal activation one segment of a straight screw is raised to the next adjacent P–N valley. The two kinks are edge by nature and can be spread out very easily. After complete spread out of the two kinks, the whole screw is brought to a new equilibrium configuration, i.e., the neighboring P–N valley. Figure 8 schematically illustrates this process. Thus the actual rate controlling process in the low temperature plastic deformation of a BCC metal is the nucleation of double-kinks. As a consequence, in contrast to FCC metals, τ^*, the thermal component of the total stress is pre-dominant at low temperatures. The strain hardening of BCC metals is relatively independent of temperature and strain rate, viz. the plastic part of stress-strain curves at different temperatures and strain rates are nearly parallel to one another. Also associated with the unique rate controlling mechanism of BCC metals is that the Cottrell–Stokes law is not obeyed, viz. the ratio of the thermal stress to the athermal stress, τ^*/τ_μ is no longer a constant. Instead, we should expect decreased τ^*/τ_μ ratio with increased plastic strain.

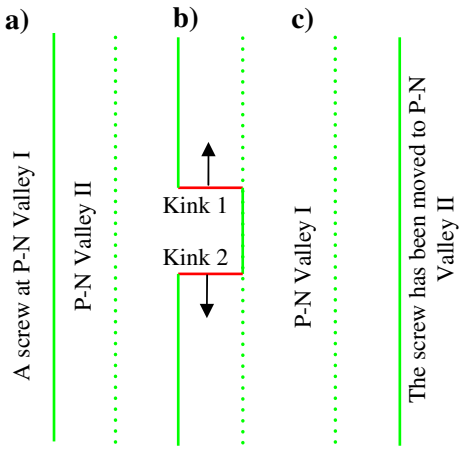

Fig. 8 Schematic illustration of the double-kink nucleation and motion in BCC lattice

In reference to Fig. 8, one can envision that the activation volume of plastic deformation of BCC metals will depend on the critical distance between the two kinks. As such, any factors that change the critical distance will change v^*. Naturally, dislocation density and grain size will impart such changes. Dorn and Rajnak [57], and many other investigators [55] have demonstrated that v^* decreases sharply with the thermal component of the stress and becomes a constant at large stresses.

The dislocation mechanisms of HCP metals are much more complicated than those of FCC and BCC metals, in that the specific operative mechanism depends on the *c*/*a* ratio (the ideal *c*/*a* ratio is 1.633), purity level and temperature [55, 56]. Three glide modes are detected in HCP metals, and they are basal slip (system (0001) $<11\bar{2}0>$), prismatic slip (system $\{10\bar{1}0\}<11\bar{2}0>$) and pyramidal slip (system $\{10\bar{1}1\}<11\bar{2}0>$). Basal slip is usually favored by HCP metals with *c*/*a* ratio larger than the ideal value. For example, below 200 °C, basal slip is the dominant mechanism for Mg. Conrad et al.[82] performed detailed study on the rate-controlling mechanism for plastic flow of Mg crystals at low temperatures, and came to the conclusion that the rate controlling mechanism is the intersection of dislocations. Conrad also studied the thermally activated deformation of α titanium at low temperatures [93], and observed strong effect of impurity atoms on the thermal activation. He reported an activation volume of $80b^3$ at τ^* = ~10 MPa, but only $8b^3$ at τ^* = ~450 MPa. He also showed that the activation volume of commercial purity α-Ti rapidly reduced to almost a constant when τ^* is beyond 50 MPa. Afterwards, it only decreases very slowly with τ^*.

Models for grain size effect on SRS

FCC metals

Conrad divided the grain size into three regimes according to the possible plastic deformation mechanisms [94]. The grain size range of each regime is: $d > 1$ μm (Regime I); 1μ m $> d >$ 10 nm (Regime II); $d <$ 10 nm (Regime III). In Regime II, he derived a response function based on thermally activated shear of individual atoms inside the grain boundary assisted by stress concentration due to ''pile-up'' of dislocations at the grain boundaries. The response function bears similarity to that of Swygenhoven et al. [95, 96], who propose that grain boundary shearing is the only operative mechanism and there is no plasticity from the grain interior. As such, the activation volume will be around $1b^3$. This is much smaller than the

experimentally measured activation volumes of this grain size regime [17, 60].

Recently, in an attempt to explain the small activation volumes and enhanced SRS of FCC metals with NC grains and nano-scale twins, Asaro and Suresh [54] have proposed a mechanistic model. The major part of their model is based on the model of Rice [97] for emission of dislocations at a crack tip due to stress concentration, and takes into account emission of partial dislocations, contribution of mechanical twinning, etc., which have been observed experimentally for some FCC metals. Their model seems to be able to give activation volumes in the range 3–10b^3. However, as pointed out by Swygenhoven et al. [98], the model of Asaro and Suresh is based on purely athermal mechanically driven nucleation and propagation of dislocations from the grain boundaries.

From Eq. (11), the SRS depends on the evolution of τ and v^* with grain size. According to Becker [99], the physical activation volume can be written as

$$v^* = b \cdot \xi \cdot l^*, \tag{21}$$

where ξ is the distance swept out by the glide dislocation during one activation event, and $l^*$is the length of dislocation segment involved in the thermal activation (or the Friedel sampling length that scales with the average contact distance between two obstacles). For CG-FCC metals with forest cutting as the dominant mechanism for thermal activation process, l^* should be roughly the average forest dislocation spacing which scales with the inverse square root of the forest density as $\rho_f^{-1/2}$. The parameter ξ may decrease slightly with the applied stress. Consequently, the activation volume will decrease with applied stress. This has been borne out by experiments on heavily deformed Cu where the activation volume is ~100b^3. If Equation (21) is substituted into (11), we have

$$m = \frac{kT}{\tau \cdot l^* \cdot \xi \cdot b}. \tag{22}$$

We assume that ξ is a constant for simplification. We will try to understand the variations of m as a function of grain size or plastic strain from the combined variation of $\tau \cdot l^*$. If we combine the Hirsch–Bailey relation with the Hall–Petch relation for the flow or yield stress of FCC metals, we have

$$\tau = \tau_0 + (\alpha\mu b\sqrt{\rho} + \frac{\beta}{\sqrt{d}}). \tag{23}$$

The first term in Eq. (23) is from the lattice friction, the second is from the Hirsch–Bailey relation and the third is the Hall–Petch relation. α and β are proportionality factors. The obstacle spacing or ''sampling length'' l^* can be viewed as having two possible limits, l_1^* and l_2^*[17]:

$$l_1^* = \frac{\eta}{\sqrt{\rho}}, \text{and} \tag{24a}$$

$$l_2^* = \chi d. \tag{24b}$$

We envisage that the ''sampling length'' defined by (24a) is likely to be the controlling length scale when the grain sizes and density of dislocations are both large, and that defined by (24b) the controlling length scale at very small grain size (and small dislocation density in the grain interior as well). The two parameters, η and χ are proportionality factors. Thus, one should anticipate that as the grain size is decreased there is a transition grain size when the controlling sampling length changes from l_1^* to l_2^*. The transition occurs when l_1^* and l_2^* are of the same order of magnitude. That is, $d_{\text{transition}} \approx 1/\sqrt{\rho}$ if assuming the two proportionality factors are also of the same order. Using typical dislocation density values in metals, $d_{\text{transition}}$ is estimated to be of the order of 10–500 nm. For conventional grain size the forest cutting is the dominant thermal activation mechanism, and we have

$$\tau \cdot l^* \cong \tau \cdot l_1^* = (\tau_0 + \alpha\mu b\sqrt{\rho} + \frac{\beta}{\sqrt{d}})(\frac{\eta}{\sqrt{\rho}}) \cong \alpha\eta\mu b + \frac{\beta\eta}{\sqrt{\rho d}}. \tag{25}$$

It follows from (22) and (25) that

$$m = \frac{kT}{\xi b} \cdot \frac{1}{\alpha\eta\mu b + \beta\eta/\sqrt{\rho d}}. \tag{26}$$

In writing (25) and (26), the lattice friction term has been dropped since it is usually very small for FCC metals. Equation (26) indicates that when the dislocation density is increased by plastic deformation in an FCC metal with a given d, the SRS should increase. This should explain the experimental observations by Zehetbauer and Seumer[76].

On the other hand, as the grain size is refined into the UFG/NC regime, the controlling sampling length may become l_2^*, and we have

$$\tau \cdot l^* \cong \tau \cdot l_2^* = (\tau_0 + \alpha\mu b\sqrt{\rho} + \frac{\beta}{\sqrt{d}}) \cdot \chi d \cong \chi\alpha\mu b\sqrt{\rho} d + \beta\chi\sqrt{d}. \tag{27}$$

And the SRS is now

$$m = \frac{kT}{\xi b} \cdot \frac{1}{\chi(\alpha\mu b\sqrt{\rho}d + \beta\sqrt{d})}. \quad (28)$$

Equation (28) suggests that when the grain size is refined into the UFG/NC regime, SRS should increase with reduced grain size. This can serve as at least a qualitative explanation for the grain size dependence of SRS of FCC metals presented in this paper (Figs. 1–4). It should be noted that cross-slip is not considered in deriving Eqs. (26) and (28). Therefore, stacking fault energy effect is not reflected in these two equations. Application of Eq. (28) to specific cases depends on a number of parameters which at this point are still to be determined. Therefore, we would rather take Eq. (28) as predicting the trend.

Very recently, based on dislocation bow-out from grain boundaries, Lian and co-workers [100] have derived an equation to associate SRS with the activation volume for NC FCC metals. First, they argued that the critical stress for the bow out of an edge dislocation source can be written as

$$\tau = \frac{0.12\mu b}{L}[\ln(\frac{L}{b}) - 1.65], \quad (29)$$

where L is the dislocation line or source length. They further took the activation volume to be Lb^2. Finally they have

$$m = \frac{\sqrt{3}kT}{\alpha\mu b^3}[\ln(\frac{v^*}{b^3}) - 1.65]^{-1}. \quad (30)$$

They showed that Eq. (30) can provide quite satisfactory fitting for a number of experimental data sets. Apparently, Eq. (30) results in a cut-off activation volume which is ~$5b^3$. Below this, the strain rate sensitivity would be negative. This cut-off activation volume needs further explanation. When the logarithmic term approaches 1.65 from either side, m will exhibit singularity. Notwithstanding this, the agreement of Eq. (30) with experimental results is impressive when v^* is larger than $10b^3$.

It is interesting to point out that Armstrong and co-workers reported grain size effect on activation volumes of FCC metals [37, 39]. They associated the thermodynamics of plastic deformation as a function of grain size in terms of the Hall–Petch parameters. The formalism of their equations bears some similarity to that of Eq. (28) in this paper.

BCC metals

For BCC metals, the activation volume decreases to nearly a constant when the stress is increased to a moderate level [55, 57]. This phenomenon can be readily understood by appealing to the double-kink nucleation process as the rate-controlling mechanism for BCC metals at low homologous temperatures. Reduction in grain size is equivalent to increasing the flow stress or yield strength according to the Hall–Petch relation. Dorn and Rajnak's analyses [57] show that the critical length of the double kink, or the spread width between the two kinks would be ~10^{-4} cm, or ~1.0 μm. Below this, the activation volume decreases with stress only very slowly. However, the stress is still following the Hall–Petch relation. If the Hall–Petch equation is inserted into Eq. (11) to replace the stress term, we have for BCC metals

$$m = \frac{kT}{(\tau_0 + k_{H-P}d^{-1/2}) \cdot v^*}. \quad (31)$$

Usually, for BCC metals, the Hall-Petch coefficient is independent both of strain rate and temperature, as well as of grain size to a large extent. Equation (31) shows that when the grain size is reduced into the UFG regime (below 1 μm, which coincides with the critical spread width of the double kinks), we anticipate reduced SRS for BCC metals. It is worthwhile pointing out that plotting Eq. (31) along with the constitutive equation for BCC Fe proposed by Jia, Ramesh and

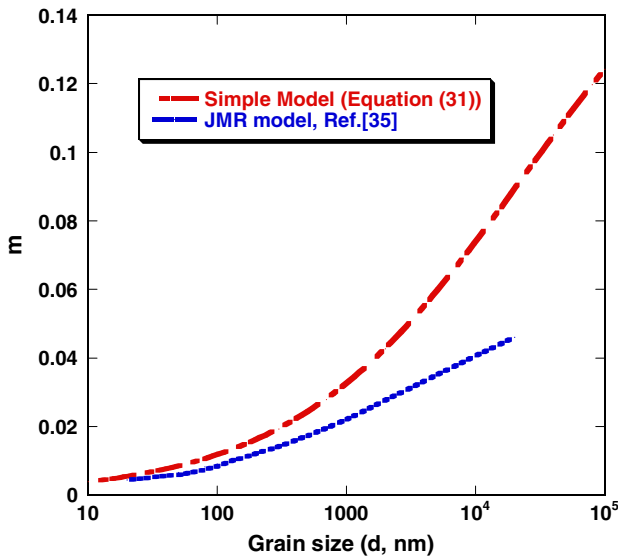

Fig. 9 Plot of the simple model for BCC metals (Eq. (31)) along with the model proposed by Jia et al. [35]

Ma[35] (see Fig. 9) indicates the two almost converge into one curve at $d < 1.0$ μm. But (31) tends to overestimate SRS at large grain size. This is understandable since at large grain size, the activation volume is larger but (31) assumes a constant value for the activation volume which is only justified for small grain sizes.

It therefore turns out that the decrease of SRS with reduction of grain size in BCC metals can be simply explained by the increasing prevalence of grain boundary strengthening, while the rate controlling mechanism stays the same, viz. nucleation of double kinks. Equation (31) can be used to describe the grain size effect on SRS in the UFG/NC regime quite satisfactorily by assuming a constant activation volume independent of grain size.

It is uncertain if double-kink nucleation will still be the rate controlling mechanism when the grain size is below 50 nm or around 10 nm. Available experimental data on fully-dense BCC metals have only been to the smallest grain size of ~80 nm. Whether grain boundary related mechanism has an effect in grain size below, for example, 50 nm, is yet an open question. Due to the fact that most BCC metals are refractory metals with high melting point and thus production of bulk nanocrystalline materials would be extremely difficult at this point, other unconventional experimental techniques, such as micro-compression [101, 102], may have to be utilized to probe the rate effect on small specimens. Therefore, new models may be needed if new experimental results contradicting the present observations become available.

HCP metals

Due to the dearth of experimental results on grain size effect on SRS of HCP metals in the UFG/NC regime, we will not proceed to discuss the possible models or theories regarding the rate controlling mechanism for HCP plastic deformation in the UFG/NC regimes. We envision more effort will surface in this area due to the rising technological importance of HCP metals such as Ti-, Be- and Mg-based alloys in many critical applications.

Significance of the strain rate effect of UFG/NC regimes in constitutive response

We anticipate that the different behavior of strain rate sensitivity of UFG/NC metals as a function of lattice structure and grain size will strongly affect the constitutive responses of the materials. Such responses include stress-strain curves, plastic instability, superplasticity and failure mode. Since plastic instability and superplasticity are two inter-related phenomena, and therefore they can be combined in the following discussion.

Under uniaxial tension, plastic instability manifests itself as necking. It occurs at the maximum load or stress. For a rate independent metal, usually Considère criterion is used to predict the point of necking, or the initiation of tensile instability [103],

$$\frac{\mathrm{d}\sigma}{\mathrm{d}\varepsilon} \leq \sigma, \quad \text{or } \gamma = \frac{1}{\sigma}\frac{\mathrm{d}\sigma}{\mathrm{d}\varepsilon} < 1, \tag{32}$$

where σ and ε are the true stress and true strain under uniaxial tension. If the plastic deformation of the metal is rate sensitive with an SRS of m, Hart derived the criterion for the tensile instability as

$$\gamma + m \leq 1, \tag{33}$$

where γ is defined in Eq. (32). Equation (33) suggests that for the rate dependent metals, the change of m as a function of grain size can impart strong effect on the constitutive response, particularly on the tensile instability behavior. The parameter γ reflects the capacity of the metal to be strain hardened. One disadvantage of UFG/NC metals is its lack of capability to store dislocations during plastic deformation, and therefore γ is usually small. This entails easy onset of tensile instability. However, for FCC metals, this can be offset by the much enhanced SRS through decreasing the grain size into the UFG/NC regime. This new property of UFG/NC FCC metals has drawn the attention of a few investigators who postulate it as one of the strategies of improving tensile ductility of UFG/NC metals [14, 104].

Jonas et al. [105], have derived a flow localization parameter under compression. This parameter, α, is a function of the strain hardening parameter, γ, and the SRS of the metal, and

$$\alpha = \frac{\gamma - 1}{m}. \tag{34}$$

Increased α points to increased propensity for flow localization or plastic instability under compression. Again, we see that for UFG/NC FCC metals, since m is elevated significantly compared to their coarse-grained counterparts, it will counteract the decreased strain hardening capacity, and retain some resistance to plastic instability. It should be kept in mind that one of the most important features of flow instability is the development of highly concentrated localized plastic deformation regions where flow rate or plastic strain

rate is many folds higher that their surroundings [106]. One should therefore expect that enhanced SRS primarily retards growth of instability by hardening these regions. In other words, the fractured specimen of UFG/NC metals should have quite small area reduction, even though the fracture surface may exhibit ductile features such as dimples [67, 107–109].

Superplasticity has been reported for UFG/NC FCC metals and alloys [110, 111]. We believe that this is at least partly due to the enhanced SRS as a consequence of refined grain size.

On the other hand, for BCC metals, experimental results presented previously in this paper show decreased SRS with reduction in grain size (Fig. 6). Such behavior will certainly bring forth strong influence on the constitutive behavior of UFG/NC BCC metals. One such influence is the increased susceptibility to flow localization under uniaxial compression simply according to Eqs. (32) and (33). For example, for UFG/NC iron produced by hot consolidation, metallic-glass-like behavior has been observed under quasi-static compression, where shear band formation and development takes over the uniform plastic flow in coarse-grained Fe [35, 112]. Figure 10 displays the quasi-static uniaxial compressive stress-strain curve of hot-consolidated UFG Fe (grain size 268 nm) [112], along with the optical micrographs of the specimen showing shear bands and their evolution. The stress-strain curve exhibits absence of work hardening. Figure 11(a) shows the bright field TEM micrograph depicting the microstructure within a shear band and its vicinity. It clearly suggests that the shear banding process involves dislocation activities and it is non-adiabatic. Diffraction pattern from grains within the shear band indicates strong texturing (Fig. 11(b)), implying geometric softening as the mechanism for the formation and development of such non-adiabatic shear band. Details of the process are still under investigation.

Under dynamic loading, most UFG/NC BCC metals exhibit adiabatic shear banding as the prevalent plastic deformation mechanism. This can be understood on the basis of mechanics and physics of adiabatic shear band for metals. For example, a simple susceptibility parameter has been derived by Wright for the occurrence of adiabatic shear banding of metals. It depends on other materials properties as [113]

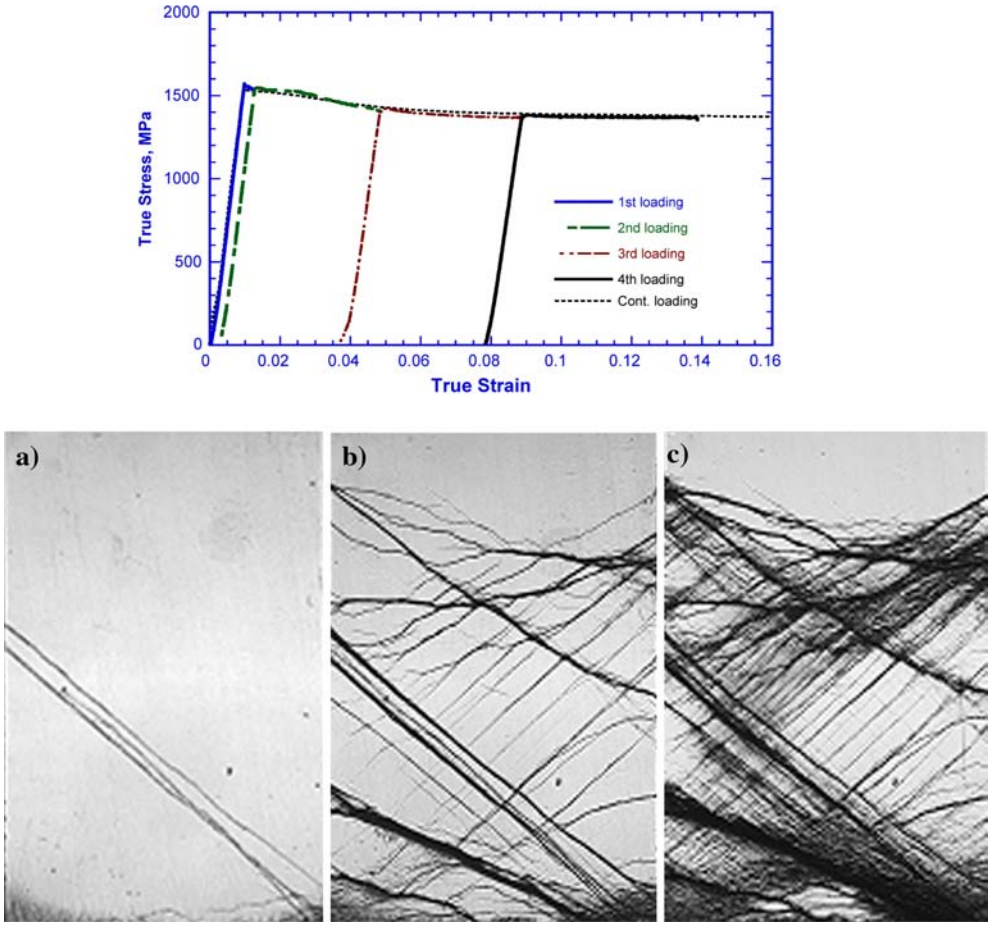

Fig. 10 Compressive uniaxial loading-unloading-reloading stress-strain curve of a consolidated ultrafine grained Fe (grain size 268 nm). The optical micrographs of (**a**), (**b**) and (**c**) correspond to the post-2nd loading, post-3rd loading and post-4th loading states, respectively. The onset and subsequent development of shear bands are clearly shown. Details can be found in Refs. [35, 112]

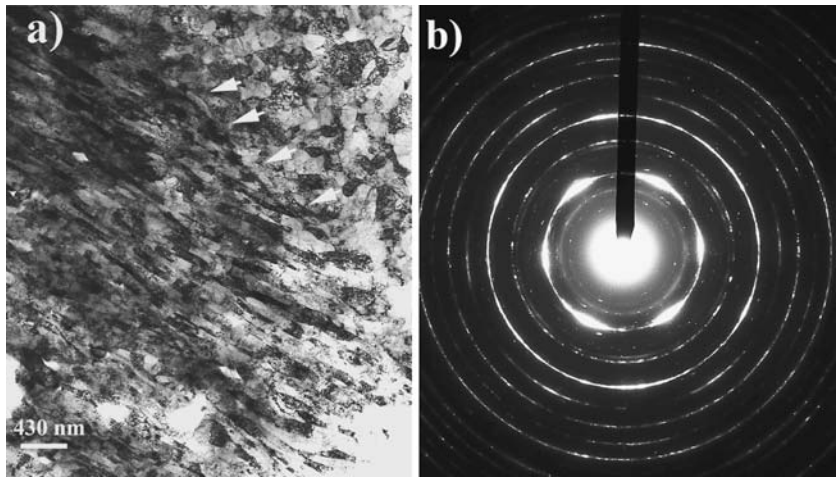

Fig. 11 Bright field TEM micrograph showing the microstructure within a shear band and its vicinity in a consolidated Fe specimen after quasi-static compression (**a**), and electron diffraction pattern from the shear band region (**b**) showing strong texturing. The Fe grains within the shear band are severely elongated, forming a sharp boundary with the surrounding equi-axed grains (the boundary is indicated by the arrows)

$$\frac{\chi_{\mathrm{ASB}}}{a/m} = \min\left\{1, \frac{1}{(n/m) + \sqrt{n/m}}\right\}, \tag{35}$$

where χ_{ASB} is the susceptibility to adiabatic shear banding, a the non-dimensional thermal softening parameter defined by $a = (-\partial\sigma/\partial T)/\rho\, c$ (σ is the flow stress, T the temperature, ρ the density and c the specific heat of the material); n is the strain hardening exponent defined by the Hollomon equation (power law hardening, or $\sigma_F = K\varepsilon^n$, where σ_F is the flow stress and K a constant) and m the SRS. For UFG/NC metals, usually strain hardening is small due to the poor capability of storing dislocations during plastic straining. Thus, the stress-strain curves exhibit elastic-nearly perfect plastic behavior, and n is approaching zero. Therefore, Eq. (35) can be re-written as [113]

$$\chi_{ASB} = \frac{a}{m} = \frac{\lambda\sigma_0}{\rho cm}, \tag{36}$$

where $\lambda = -(1/\hat{\sigma}_0)(\partial\sigma/\partial T)$ is the thermal softening parameter evaluated under isothermal conditions ($\hat{\sigma}_0$ is a normalizing stress), and σ_0 is the yield strength. Equation (35) indicates that elevated yield strength combined with much reduced SRS of UFG/NC metals with BCC lattice structures should drive the metals more prone to adiabatic shear banding. This has indeed been verified in a number of BCC metals with UFG/NC microstructure. For example, commercial purity Fe with UFG microstructure was processed by ECAP for four passes and then loaded under uniaxial dynamic compression. Figure 12 displays the post-loading scanning electron micrograph showing localized shearing, indicating the occurrence of adiabatic shear banding during dynamic loading. If the grain size is further refined through SPD at a lower temperature, adiabatic shear banding is more pronounced (under dynamic loading), as shown in Fig. 13. Here the plastic deformation is concentrated into two sets of adiabatic shear bands. Within the shear band, plastic flow of the material is much more severe than the adjacent area. This severe plastic flow is accompanied by considerable temperature rise, a typical feature associated with adiabatic shear banding [113].

Another important example is the adiabatic shear banding in UFG/NC tungsten. Due to its high mass density and high strength, W has been investigated in the past few decades to replace depleted uranium for kinetic energy (KE) penetrator material [114]. One of the critical requirements for KE penetrator is the so-called self-sharpening effect which enables the penetrator head to remain sharp during the course of target penetration. The self-sharpening effect is rooted in the

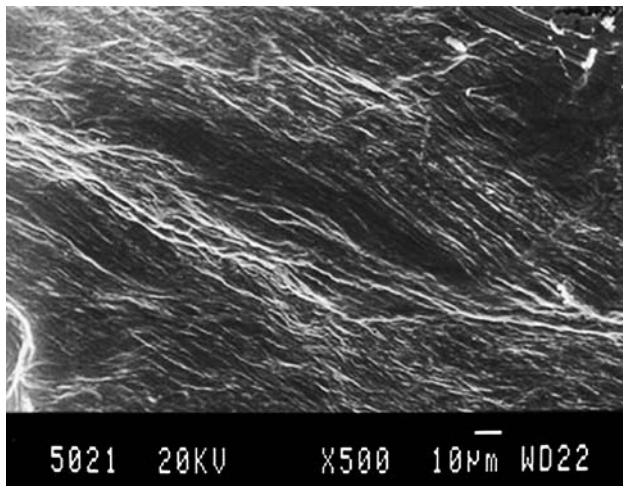

Fig. 12 Scanning electron micrograph of post-dynamic loading ECAP Fe showing localized shearing. Details can be found in Ref. [33]

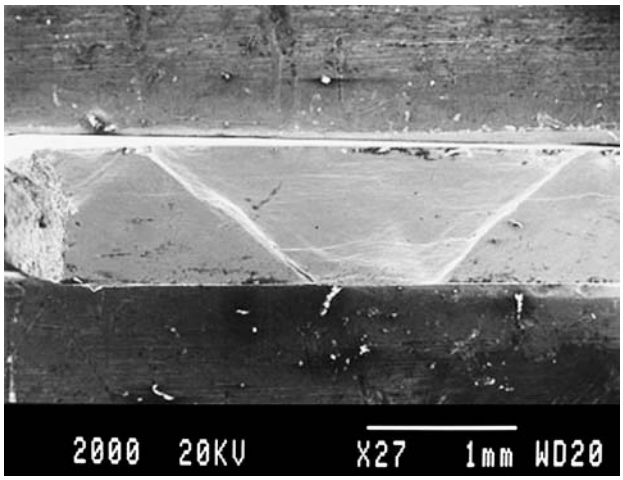

Fig. 13 Scanning electron micrograph of ECAP and low temperature rolled Fe after uniaxial dynamic compression showing severely localized deformation. Formation of adiabatic shear bands is obvious. Details can be found in Ref. [33]

material's strong propensity for adiabatic shear banding so that material is discarded away in a localized fashion, forming a small channel of penetration. Conventional coarse-grained W is strongly resistant to adiabatic shear banding, mainly because of its ceramic-like brittle fracture under mechanical loading [32]. By SPD processing, the grain size of W can be refined into UFG/NC regime. Interestingly, not only can the strength level be considerably increased, but the SRS is also reduced and the ductility is much improved. The experimental details, results and explanations can be found in Refs. [32, 34, 79]. As a result, adiabatic shear bands have been observed for the first time in commercial purity tungsten. Figure 14 shows the optical micrograph of adiabatic shear bands from a UFG W after uniaxial dynamic compression. As a consequence of the severe adiabatic shearing, a crack is formed within the shear band (Fig. 14 (b)). Also the dynamic stress-strain curves of the UFG W specimens show significant softening after certain plastic strain, a result from adiabatic shear banding (Fig. 15) [32]. If the grain size is further refined into the nanocrystalline regime by high-pressure torsion, this behavior becomes more noticeable (Fig. 16) [79]. First, the width of adiabatic shear band becomes narrower than that of the UFG W (~5 μm in NC W (Fig. 17 (b)) versus ~40 μm in UFG W (Fig. 14 (b))). Secondly, the stress drop in the stress-strain curves comes in earlier than that of the UFG W (Fig. 15 vs. Fig. 16). Based on these experimental observations of the constitutive behavior of UFG/NC BCC metals, we believe that hope is looming for the make of W penetrators with excellent performance [115].

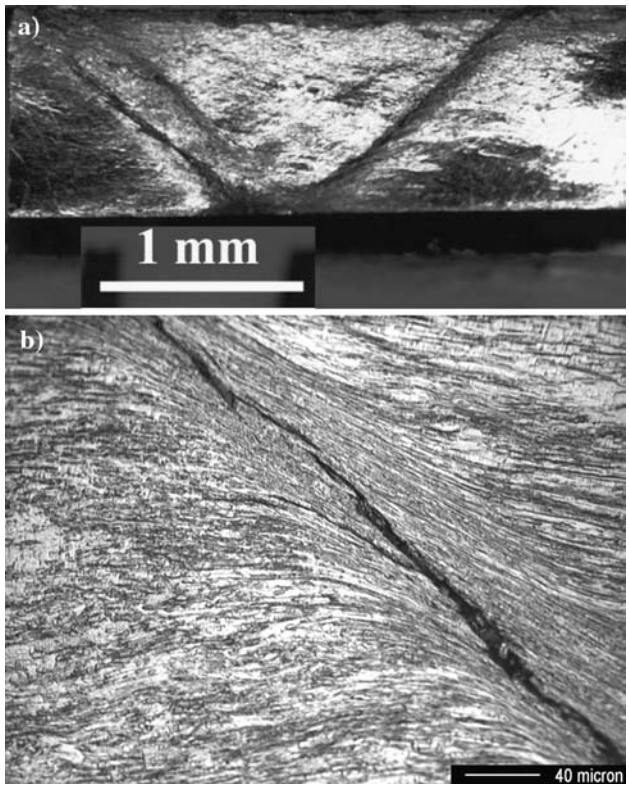

Fig. 14 Adiabatic shear bands in UFG W (**a**) after uniaxial dynamic compression. In (**b**), the microstructure of the adiabatic shear band is revealed by polishing and etching. Also seen in (**b**) is a crack as the result of adiabatic shearing

On the other hand, under dynamic loading, UFG/NC metals with FCC lattice may exhibit different behavior from their BCC counterparts according to Eq. (35). A significantly enhanced SRS in FCC UFG/NC metals may balance the elevated yield strength,

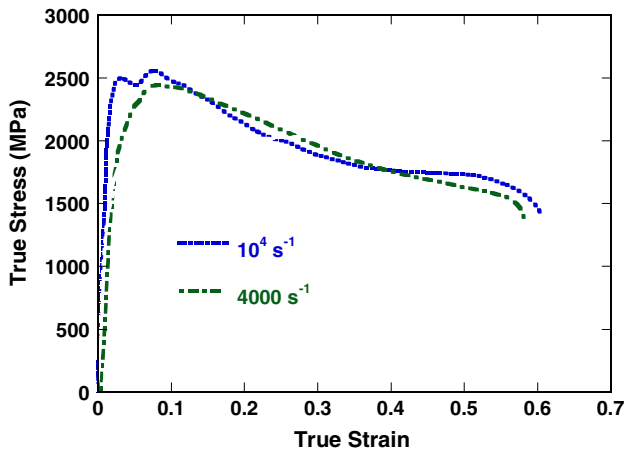

Fig. 15 Uniaxial dynamic compressive stress-strain curves of UFG W. Strain softening is obvious. Details can be found in Refs. [32, 34]

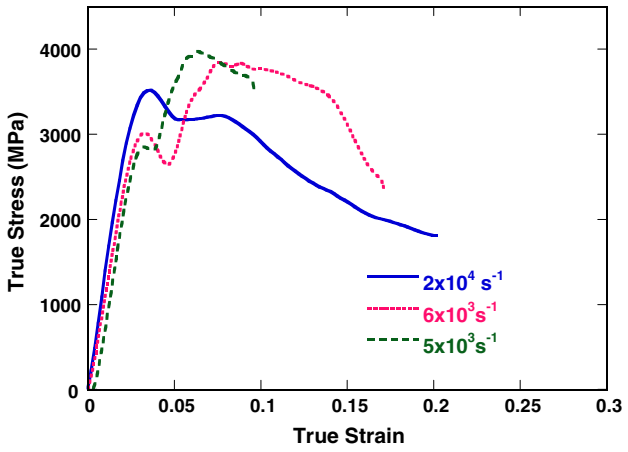

Fig. 16 Uniaxial dynamic stress-strain curves (compression) of NC W. Details can be found is Ref. [79]

imparting inconsequential increase in χ_{ASB}. This will render dynamic behavior of UFG/NC metals not so different from the coarse-grained counterparts.

In summary, different SRS behavior in the UFG/NC regime for metals with different lattice structures brings forth remarkably different constitutive responses under various loading conditions. Major influence of change in SRS with grain size reduction is on the plastic instability and failure mode of the metals. For FCC metals with UFG/NC microstructure, enhanced SRS will increase its resistance to necking under tension and its resistance to adiabatic shear banding under dynamic compression. For BCC metals with UFG/NC microstructure, reduced SRS renders the metals more prone to plastic instability. This behavior happens to be a long-sought after property for some critical applications.

Outstanding issues and future direction

While great progresses have been made in the past few years to understand the strain rate effect and its influence on the constitutive response in the UFG/NC regime, there remain many issues that call for further effort.

First, experimental data is lacking for HCP metals with UFG/NC microstructure, some of which are becoming increasingly important in today's technology. For example, two important ultra-light metals, Mg and Be, have HCP structure. The work on another important HCP metal, Ti, is also very limited. Systematic work is needed to understand the strain rate effect in those HCP metals with UFG/NC microstructures, including experiments and theoretical or numerical consideration.

Secondly, for BCC metals, the lower bound of the UFG/NC regime has not been reached yet. The absolute majority of data for BCC metals are on the upper bound of the NC regime (grain size > 100 nm). What will happen if the grain size of BCC metals is driven below 50 nm is still an open issue. Whether double-kink mechanism will be the operative and the rate controlling mechanism needs to be clarified. When the grain size is below 50 nm, grain boundary activities may not be excluded from the contributing mechanisms. If so, an increased SRS in NC BCC metals should be anticipated. However, due to the difficulty in producing fully dense NC BCC metals, alternatives may be attempted such as the use of small samples, nanoindentation on fully dense thin film specimens, etc. Furthermore, theoretical work or numerical simulations will be needed for NC BCC metals (grain size below 50 nm).

Thirdly, detailed and plausible theories and models are needed for FCC metals to explain the wealth of experimental results on strain rate effect in the UFG/NC regime. For example, the role of stacking fault energy has not been considered yet in existing models. Even though microsized or nanosized twinning is observed to enhance SRS of Cu, a convincing model is still waiting to be proposed. The role of cross-slip, a thermally activated process, has not yet been studied in

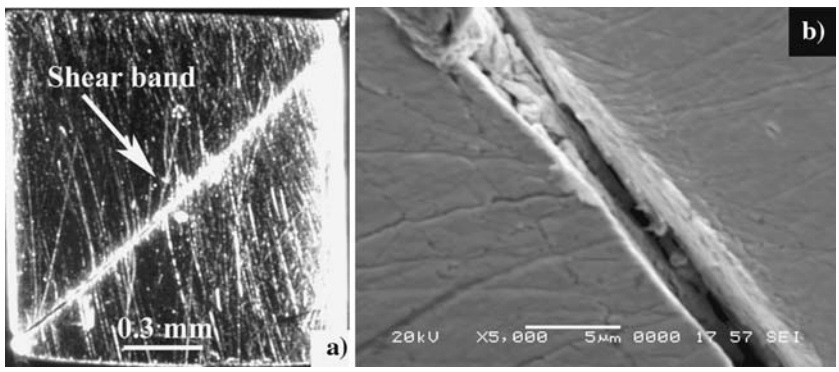

Fig. 17 Optical micrograph of adiabatic shear band in NC-W (**a**) and the scanning electron micrograph of the shear band (**b**). The crack is a result of severely localized shearing during dynamic compression

terms of its effect on strain rate effect in the UFG/NC regime.

Finally, the link between the Hall-Petch parameters and the strain rate effect needs to be established on firm grounds. It was believed that the same mechanisms that affect the Hall–Petch parameters, particularly the Hall–Petch coefficient, $k_{H\text{-}P}$, may control the strain rate effect as a function of grain size [37].

Concluding remarks

A critical review is provided with regard to the strain rate effect in the ultrafine-grain and nanocrystalline regimes, and its influence on some constitutive responses of UFG/NC metals with different lattice structures. Consistent experimental results indicate that strain rate sensitivity of FCC metal has been remarkably enhanced in the UFG/NC regime, while that of BCC metals has been considerably reduced. No convincing conclusion can be drawn for HCP metals due to lack of reliable experimental data.

For FCC metals, a transition in the controlling sampling length for dislocation mechanism may be used to explain the observed experimental results. For BCC metals, the reduced strain rate sensitivity in the UFG/NC regime can be simply considered to be due to the increasing part of the total stress due to the Hall–Petch strengthening. Equations are derived for FCC and BCC metals which can serve as at least qualitatively predicting the trend in either case.

The opposite changes of strain rate effect as a function of grain size in FCC and BCC metals bring forth remarkably different influence on the constitutive responses on the two lattice structures in the UFG/NC regime. For FCC metals, enhanced strain rate sensitivity compensates for the reduced strain hardening effect. This can be used as a strategy to improve tensile ductility of UFG/NC metals. On the other hand, reduced strain rate sensitivity of UFG/NC BCC metals entails strong propensity for plastic instability under mechanical load. This constitutive response happens to be a long-sought-after property for a number of critical applications. Outstanding issues that need further effort are briefly discussed.

Acknowledgments The author is indebted to Professors E. Ma and K. T. Ramesh (Johns Hopkins University) for many illuminating discussions. He is also grateful to Dr. T. W. Wright (US Army Research Lab) for his help in the understanding of the physics and mechanics of adiabatic shear banding. Dr. L. Magness has kindly offered assistance to the author with his knowledge about penetrator performance. Some experimental results presented in this article were obtained at JHU-CAMCS through the support by ARL under the ARMAC-RTP Cooperative Agreement #DAAD19-01-2-0003. Many former colleagues participated in the experimental work, and the author would like to extend his gratitude to Drs. T. Jiao, H.T. Zhang, Y. L. Li, L. J. Kecskes, and Mr. B. E. Schuster. Finally, the author is thankful to Dr. Y. T. Zhu for inviting the author to write this article for the special issue of the Journal of Materials Science.

References

1. Hall EO (1951) Proce Phys Soc B, Lond 64:747
2. Petch NJ (1953) J Iron Steel Institute 174:25
3. Armstrong RW (1967) In: Rosenfield AR, Hahn GT, Bement ALJ, Jaffee RI (eds) Dislocation dynamics. McGraw-Hill Book Company, NewYork, p 293
4. Li JCM (1963) Trans Metal Soc AIME 227:239
5. Ashby MF (1970) Philos Mag 21:399
6. Volpp T, Goring E, Kuschke W-M, Arzt E (1997) Nanostruct Mater 8:855
7. El-Sherik AM, Erb U, Palumbo G, Aust KT (1992) Scripta Mater 27:1185
8. Schuh CA, Nieh TG, Yamasaki T (2002) Scripta Mater 46:735
9. Koch CC, Narayan J (2001) The inverse Hall–Petch effect-Fact or Artifact? presented at Structure and mechanical properties of nanophase materials-theory and computer simulations v.s.experiments. Boston MA, USA
10. Nieh TG, Wadsworth J (1991) Scripta Metallurgica et Materialia 25:955
11. Meyers MA, Mishra A, Benson DJ (2006) Progr Mater Sci 51:427
12. Koch CC (2002) Nanostructured materials: processing, properties and potential Norwich, Noyes Publications
13. Valiev RZ, Islamgaliev RK, Alexandrov IV (2000) Progr Mater Sci 45:103
14. Ma E (2006) JOM 58:49
15. Carreker RP Jr, Hibbard Jr WR (1953) Acta Metallurgica 1:657
16. Schwaiger R, Moser B, Dao M, Chollacoop N, Suresh S (2003) Acta Mater 51:5159
17. Wei Q, Cheng S, Ramesh KT, Ma E (2004) Mater Sci Eng A 381:71
18. Lu L, Li SX, Lu K (2001) Scripta Mater 45:1163
19. Hollang L, Thiele E, Holste C, Brunner D (2003) ''The influence of temperature and strain rate on the flow stress of ECAP nickel,'' presented at 2nd International Conference on Nanomaterials by Severe Plastic Deformation
20. Chen J, Shi YN, Lu K (2005) J Mater Res 20:2955
21. Han BQ, Huang JY, Zhu YT, Lavernia EJ (2006) Scripta Mater 54:1175
22. Duhamel C, Guerin S, Hytch MJ, Champion Y (2005) Deformation behavior and strain rate sensitivity of nanostructured materials at moderate temperatures. presented at Mechanical properties of nanostructured materials-experiments and modelling: MRS Symp. Proc San Francisco, CA
23. Torre FD, Van Swygenhoven H, Victoria M (2002) Acta Mater 50:3957
24. Torre FD, Spatig P, Schaublin R, Victoria M (2005) Acta Mater 53:2337
25. Kumar KS, Van Swygenhoven H, Suresh S (2003) Acta Mater 51:5743
26. Kumar KS, Suresh S, Chisholm MF, Horton JA, Wang P (2003) Acta Mater 51:387

27. Li YJ, Zeng XH, Blum W (2004) Acta Mater 52:5009
28. Li YJ, Valiev RZ, Blum W (2005) Mater Sci Eng A 410–411:451
29. Wang YM, Ma E (2003) Appl Phys Lett 83:3165
30. Wei Q, Jiao T, Mathaudhu SN, Ma E, Hartwig KT, Ramesh KT (2003) Mater Sci Eng A 358:266
31. Wei Q, Jiao T, Ramesh KT, Ma E (2004) Scripta Mater 50:359
32. Wei Q, Jiao T, Ramesh KT, Ma E, Kecskes LJ, Magness L, Dowding RJ, Kazykhanov VU, Valiev RZ (2006) Acta Mater 54:77
33. Wei Q, Kecskes LJ, Jiao T, Hartwig KT, Ramesh KT, Ma E (2004) Acta Mater 52:1859
34. Wei Q, Ramesh KT, Ma E, Kesckes LJ, Dowding RJ, Kazykhanov VU, Valiev RZ (2005) Appl Phys Lett 86:101907
35. Jia D, Ramesh KT, Ma E (2003) Acta Mater 51:3495
36. Jang D, Atzmon M (2003) J Appl Phys 93:9282
37. Rodriguez P (2004) Metall Mater Trans A 35:2697
38. Rodriguez P, Ray SK (1988) Bull Mater Sci 10:133
39. Armstrong RW (1973) J Sci Industrial Res 32:591
40. Armstrong RW (1997) –531 50:521
41. Jia D, Wang YM, Ramesh KT, Ma E, Zhu YT, Valiev RZ (2001) Appl Phys Lett 79:611
42. Hwang S, Nishimura C, McCormick PG (2001) Scripta Mater 44:1507
43. Zhang X, Wang H, Scattergood RO, Narayan J, Koch CC, Sergueeva AV, Mukherjee A (2002) Acta Mater 50:4823
44. Zhang X, Wang H, Scattergood RO, Narayan J, Koch CC, Sergueeva AV, Mukherjee A (2002) Appl Phys Lett 81:823
45. Conrad H, Narayan J (2002) Acta Mater 50:5067
46. Karimpoor AA, Erb U, Aust KT, PalumboG (2003) Scripta Mater 49:651
47. Kocks UF, Argon AS, Ashby MF (1975) Progr Mater Sci 19:1
48. Chen J, Lu L, Lu K (2006) Scripta Mater 54:1913
49. Hoppel HW, May J, Goken M (2004) Adva Eng Mater 6:781
50. Hoppel HW, May J, Eisenlohr P (2005) Zeit fur Metallkunde 96:566
51. May J, Hoppel HW, Goken M (2005) Scripta Mater 53:189
52. Witkin D, Han BQ, Lavernia EJ (2005) J Mater Eng Perfor 14:519
53. Torre FD, Pereloma EV, Davies CHJ (2006) Acta Mater 54:1135
54. Asaro RJ, Suresh S (2005) Acta Mater 53:3369
55. Conrad H (1965) In: Zackey VF (ed) High-strength materials. New York, Wiley, p 436
56. Dorn JE, Mitchell JB (1965) In: Zackey VF (ed) High-strength materials. New York, John Wiley & Sons, Inc., p 510
57. Dorn JE, Rajnak S (1964) Trans Metall Soc AIME 230:1052
58. Gupta I, Li JCM (1970) Metall Trans 1:2323
59. Dieter GE (1986) Mechanical metallurgy, 3rd edn. New York, McGraw-Hill
60. Wang YM, Hamza AV, Ma E (2006) Acta Mater 54:2715
61. Follansbee PS (1985) In: ASM Metals Handbook, vol 8: American Society of Metals, p 190
62. Elmustafa AA, Tambwe MF, Stone DS (2002) ''Activation volume analysis of plastic deformation in fcc materials using nanoindentation,'' presented at Surface Engineering 2002-Synthesis, Characterization and Applications, MRS Fall Meeting, Boston, MA
63. Valiev RZ, Alexandrov IV, Zhu YT, Lowe TC (2002) J Mater Res 17:5
64. Gray III GT, Lowe TC, Cady CM, Valiev RZ, Aleksandrov IV (1997) Nanostruct Mater 9:477
65. Wang YM, Ma E (2004) Appl Phys Lett 85:2750
66. Li YJ, Blum W (2005) Phys Status Solidi A 202:R119
67. Cheng S, Ma E, Wang YM, Kecskes LJ, Youssef KM, Koch CC, Trociewitz UP, Han K (2005) Acta Mater 53:1521
68. Lu L, Schwaiger R, Shan ZW, Dao M, Lu K, Suresh S (2005) Acta Mater 53:2169
69. Jiang ZH, Liu XL, Li GY, Jiang Q, Lian JS (2006) Appl Phys Lett 88:143115
70. Gu CD, Lian JS, Jiang ZH, Jiang Q (2006) Scripta Mater 54:579
71. Pan D, Nieh TG, Chen MW (2006) Appl Phys Lett 88:161922
72. Miyamoto H, Ota K, Mimaki T (2006) Scripta Mater 54:1721
73. Hoppel HW, May J, Eisenlohr P, Goken M (2005) Zeit fur Metallkunde 96:566
74. Kalkman AJ, Verbruggen AH, Radelaar S (2002) J Appl Phys 92:6612
75. Hayes RW, Witkin D, Zhou F, Lavernia EJ (2004) Acta Mater 52:4259
76. Zehetbauer M, Seumer V (1993) Acta Metallurgica et Materialia 41:577
77. Malow TR, Koch CC, Miraglia PQ, Murty KL (1998) Mater Sci Eng A 252:36
78. Jang D, Atzmon M (2006) J Appl Phys 99:083504
79. Wei Q, Zhang H, Schuster BE, Ramesh KT, Valiev RZ, Kecskes LJ, Dowding RJ (2006) Acta Mater 54:4079
80. May J, Hoppel HW, Goken M (2006) Mater Sci Forum 503–504:781
81. Sastry DH, Prasad YVRK, Vasu KI (1970) Metall Trans 1:1827
82. Conrad H, Hays L, Schoeck G, Wiedersich H (1961) Acta Metall 9:367
83. Trojanova Z, Lukac P, Szaraz Z (2005) Rev Adva Mater Sci 10:437
84. Cottrell AH (2002) In: Nabarro FRN, Duesbery MS (eds) Dislocations in solids, vol 11. Elsevier, p vii
85. Nabarro FRN (1987) Theory of crystal dislocations New-York, Dover
86. Cottrell AH, Stokes RJ (1955)Proce Roy Soc A 233
87. Bailey JE, Hirsch PB (1960) Philosoph Maga 5:485
88. Basinski ZS (1959) Philosoph Maga 4:393
89. Narutani T, Takamura J (1991) Acta Metallugica et Materialia 39:2037
90. Keh AS, Weissmann S (1963) In: Thomas G, Washburn J (eds) Electron microscopy and strength of crystals. New York, Interscience, p 231
91. Christian JW (1983) Metall Trans A 14:1237
92. Duesbery MS, Vitek V (1998) Acta Mater 46:1481
93. Conrad H (1967) 4 TM Canadian. J Phys 45:581
94. Conrad H (2003) Mater Sci Eng A 341:216
95. Van Swygenhoven H, Caro A (1998) Phys Rev B 58:11246
96. Van Swygenhoven H, Spaczer M, Caro A, Farkas D (1999) Phys Rev B 60:22
97. Rice JR (1992) J Mech Phys Solids 40:239
98. Van Swygenhoven H, Derlet PM, Froseth A (2006) Acta Mater 54:1975
99. Cahn JW, Nabarro FRN (2001) Philosoph Maga A 81:1409
100. Lian JS, Gu CD, Jiang Q, Jiang ZH (2006) J Appl Phys 99:076103
101. Zhang H, Schuster BE, Wei Q, Ramesh KT (2006) Scripta Mater 64:181
102. Schuster BE, Wei Q, Zhang H, Ramesh KT (2006) Applied physics letters 88:103112
103. Hart EW (1967) Acta Metall 15:351
104. Wang YM, Ma E (2004) Acta Mater 52:1699

105. Jonas JJ, Holt RA, Coleman CE (1976) Acta Metallurgica 24:911
106. Tvergaard V, Needleman A (1993) Proce Roy Soc Lond 443A:547
107. Li HQ, Ebrahimi F (2004) Appl Phys Lett 84:4307
108. Iwasaki H, Higashi K, Nieh TG (2004) Scripta Mater 50:395
109. Li H, Ebrahimi F (2006) Acta Materialia 54:2877–2886
110. McFadden SX, Mishra RS, Valiev RZ, Zhilyaev AP, Mukherjee A (1999) Nature 398:684
111. McFadden SX, Zhilyaev AP, Mishra RS, Mukherjee A (2000) Mater Lett 45:345
112. Wei Q, Jia D, Ramesh KT, Ma E (2002) Appl Phys Lett 81:1240
113. Wright TW (2002) The physics and mathematics of adiabatic shear bands. Cambridge Press
114. Magness LS (2002) ''An overview of the penetration performances of tungsten and depleted uranium alloy penetrators: ballistic performances and metallographic examinations,'' presented at 20th International Symposium on Ballistics, Orlando, Florida
115. Wei Q, Ramesh KT, Schuster BE, Kecskes LJ, Dowding RJ (2006) JOM 58:40